Understanding the Reactivity of Supported Late Transition Metals on a Bare Anatase (101) Surface: A Periodic Conceptual DFT Investigation

Xavier Deraet, Jan Turek, Mercedes Alonso, Frederik Tielens, Bert M Weckhuysen, Monica Calatayud, Frank de Proft

▶ **To cite this version:**

Xavier Deraet, Jan Turek, Mercedes Alonso, Frederik Tielens, Bert M Weckhuysen, et al.. Understanding the Reactivity of Supported Late Transition Metals on a Bare Anatase (101) Surface: A Periodic Conceptual DFT Investigation. ChemPhysChem, In press, ⟨10.1002/cphc.202200785⟩. ⟨hal-03976035⟩

HAL Id: hal-03976035

https://hal.science/hal-03976035v1

Submitted on 6 Feb 2023

HAL is a multi-disciplinary open access archive for the deposit and dissemination of scientific research documents, whether they are published or not. The documents may come from teaching and research institutions in France or abroad, or from public or private research centers.

L'archive ouverte pluridisciplinaire **HAL**, est destinée au dépôt et à la diffusion de documents scientifiques de niveau recherche, publiés ou non, émanant des établissements d'enseignement et de recherche français ou étrangers, des laboratoires publics ou privés.

HAL Authorization

Understanding the Reactivity of Supported Late Transition Metals on a Bare Anatase (101) Surface: A Periodic Conceptual DFT Investigation

Xavier Deraet,[a] Jan Turek,[a] Mercedes Alonso,[a] Frederik Tielens,[a] Bert M. Weckhuysen,[b] Monica Calatayud,[c] Frank De Proft,[*,a]

[a] Department of General Chemistry (ALGC), Vrije Universiteit Brussel (VUB), Pleinlaan 2, 1050 Elsene, Brussels, Belgium

[b] Inorganic Chemistry and Catalysis Group, Debye Institute for Nanomaterials Science, Utrecht University, Universiteitsweg 99, 3584 CG Utrecht, the Netherlands

[c] Sorbonne Université, CNRS, Laboratoire de Chimie Théorique, LCT, F. 75005, Paris, France

Corresponding author: Prof. Frank De Proft (fdeprof@vub.be)

Abstract

The rapidly growing interest for new heterogeneous catalytic systems providing high atomic efficiency along with high stability and reactivity triggered an impressive progress in the field of single-atom catalysis. Nevertheless, unravelling the factors governing the interaction strength between the support and the adsorbed metal atoms remains a major challenge. Based on periodic Density Functional Theory (DFT) calculations, this paper provides insight into the adsorption of single late transition metals on a defect-free anatase surface. The obtained adsorption energies fluctuate, with the exception of Pd, between -3.11 and -3.80 eV and are indicative of a strong interaction. Depending on the considered transition metal, we could attribute the strength of this interaction with the support to: *i*) an electron transfer towards anatase (Ru, Rh, Ni), *ii*) *s-d* orbital hybridisation effects (Pt), or *iii*) a synergistic effect between both factors (Fe, Co, Os, Ir). The driving forces behind the adsorption were also found to be strongly related to Klechkowsky's rule for orbital filling. In contrast, the deviating behaviour of Pd is most likely associated with the lower dissociation enthalpy of the Pd-O bond. Additionally, the reactivity of these systems was evaluated using the Fermi weighted density of states approach. The resulting softness values can be clearly related to the electron configuration of the catalytic systems as well as with the net charge on the transition metal. Finally, these indices were used to construct a model that predicts the adsorption strength of CO on these anatase-supported *d*-metal atoms. The values obtained from this regression model show, within a 95% probability interval, a correlation of 84% with the explicitly calculated CO adsorption energies.

Introduction

The Haber-Bosch and Ostwald processes for the production of ammonia and nitric acid, Ziegler-Natta polymerizations or cracking of hydrocarbons are just a few of the industrial applications making use of heterogeneous catalysts. In general, 80 to 90% of the total industrial production of bulk chemicals[1] or 35% of the world's gross domestic product[2] rely on such metal supported catalysts. Despite their obvious importance, some concerns regarding their economic and ecological cost as well as the continuously decreasing abundancy of these metals have triggered a rising interest for the development of new catalytic systems.[3] In addition to the excellent stability and activity, these new catalysts should exhibit maximum atom efficiency. This property describes the amount of transition metal atoms that comprise the active site and also actively

contribute to the interactions with reactant molecules.[4] As the number of reactive atoms on the outer surface of a supported nanoparticle decreases with increasing volume, the atom efficiency of large catalytic complexes will be much lower as compared to the smaller systems.[4] Hence, the prototype of such an atom-efficient heterogeneous catalyst consists of isolated single metal atoms dispersed on a support without any spatial order. The catalytic activity of these single-atom catalysts (SACs) should mainly originate from the individual metal atoms, though nearby atoms or functional groups belonging to the support can also contribute.[5]

However, the systematic reduction in size of the catalytic system triggers undesired deactivation processes such as sintering or clustering due to the more pronounced mobility of atoms with respect to nanoparticles.[6] Therefore, a significant part of SAC development involves a careful selection of supports that offer a strong anchoring point for the metal without drastically affecting its reactivity.[7] The strength of the interaction between a single metal atom and the support appears to be primarily dictated by a range of structural and electronic parameters, depending on the properties of the metal as well as the oxide support. Herein, we investigate the adsorption and reactivity of *d*-transition metals on a defect-free anatase surface, a polymorph of titanium dioxide (TiO_2). This oxide surface is a representative example of a highly interacting surface which owes this property to the reducible nature of its Ti^{4+} ions. Next to the reducible nature, anatase exhibits very strong (photo)catalytic properties,[8] despite not being the most thermodynamically stable crystalline form of TiO_2.[9] Consequently, anatase-supported transition metals constitute important heterogeneous catalytic systems in many reactions.[10]

Based on existing computational ab initio studies, the adsorption of single *d*-metal atoms on reducible surfaces,[11,12] such as the considered anatase or ceria (CeO_2) support, is systematically associated with adsorption energies that are significantly stronger than in the case of more inert surfaces.[13] This finding is invariably ascribed to the potential charge transfer from the *d*-metal to the reducible oxide surface and the ensuing formation of a strong interaction between an oxidized transition metal and O^{2-} atoms of the surface. In the case of non-reducible supports, the metal-support interactions are often attributed to a combination of van der Waals dispersion, polarization and orbital mixing effects.[13,14] Furthermore, it was observed that the adsorption of late transition metal atoms of Group 8-10 on the amorphous silica support was strongly driven by the oxophilicity of the *d*-metal. As such, the tendency of the transition metal to form strong ionic bonds with O^{2-} atoms of the surface was found to be associated with a weaker adsorption on the non-reducible support.[14] Additionally, the possible rearrangement of the electronic configuration of the *d*-metal upon adsorption, allowing outer *s* electrons of the transition metal to be promoted into the incomplete *d* shell, also appears to have a positive influence on the interaction strength. This was observed for adsorption on both reducible and non-reducible supports.[11-14] Aside from charge transfer and orbital effects, trends in adsorption energies have also already been assigned to the extent to which the support is geometrically deformed upon interaction as well as to the number of available *d* electrons of the transition metal.[11e]

In contrast to the widely available data on the driving forces behind specific adsorption processes, comprehensive reactivity studies of SAC systems are lacking. However, a systematic and fundamental approach can provide crucial insights into computed mechanisms or experimentally obtained selectivity and product ratios. In a previous paper describing the adsorption and reactivity of single late transition metals on non-reducible amorphous silica, the conceptual

Density Functional Theory (CDFT) reactivity indices showed that the catalytic activity was nearly completely governed by the inherent chemical properties of the transition metal.[14] Based on these findings, we aim in this work at demonstrating the influence of a reducible oxide support, and hence the associated charge transfer process between the *d*-metal and oxide surface, on the reactivity of the catalytic complex. The strength of the CDFT descriptors resides in their ability to reveal the orbital- or electrostatic-controlled reactivity of the catalytic system without having to model the interactions with external reagents. Furthermore, they also enable different sites of a surface to be distinguished according to their preference for either a charge transfer-based interaction (soft system) or rather an electrostatic one (hard system). Consequently, a systematic study of CDFT descriptors for different supports, transition metals and cluster sizes should reveal a series of valuable trends in reactivity, which might serve as an insightful and predictive tool for experimental understanding of new catalytic systems.

Computational Details

Construction of the (101) Low-Index Plane of the Anatase Surface

Starting from crystallographic data,[15] the anatase unit cell was optimised using periodic, spin-polarized DFT calculations as implemented in the Vienna Ab Initio Simulation Package (VASP 5.4.4).[16] The titanium and oxygen atoms were respectively characterised by 12 and 6 valence electrons, corresponding to a $[Ne]3s^2 3p^6 4s^2 3d^2$ and $[He]2s^2 2p^4$ electron configuration. The interactions between the explicitly treated valence electrons and the ionic cores were described using the Projector-Augmented-Wave (PAW) method.[17] The tetragonal unit cell of anatase consisting of 12 atoms (4 Ti and 8 O atoms) with experimental lattice parameters[18] of a = 3.785 Å and c = 9.512 Å was optimised with the PBE[19] functional and the Grimme DFT-D3 empirical dispersion with the Becke-Johnson (BJ) damping function.[20] In analogy with a previous work on anatase,[21] an effective Hubbard term[22] of 4 eV, acting solely on the 3*d* shell of titanium atoms, was introduced to correct for the inappropriate description of band gaps with GGA functionals. The optimised unit cell geometry was subsequently subjected to a sequence of volume scaling, enabling the determination of the equilibrium volume (V_0) through the fitting of the Birch-Murnaghan equation of state.[23] The most suitable energy cut-off and Monkhorst-Pack k-point grid density[24] was determined based on a benchmark study, for which the results are summarized in Figures S1 and S2 as well as Table S1 of the Supporting Information. This revealed an expansion of wave functions up to a kinetic energy of 500 eV in combination with a (9 x 9 x 3) grid to be the most appropriate approach for our system. The calculated lattice parameters are fully in line with previous DFT+U calculations[25] and the obtained deviation in the lattice parameter ratio (c/a) only amounts to 0.44% in comparison with experimental data[18] (see Table S2 of the Supporting Information for more details). Ultimately, this bulk structure with a = 3.860 Å and c = 9.743 Å was used to construct a (3 x 1) periodic supercell of the desired (101) anatase surface slab consisting of 6 Ti-layers (Figure 1).

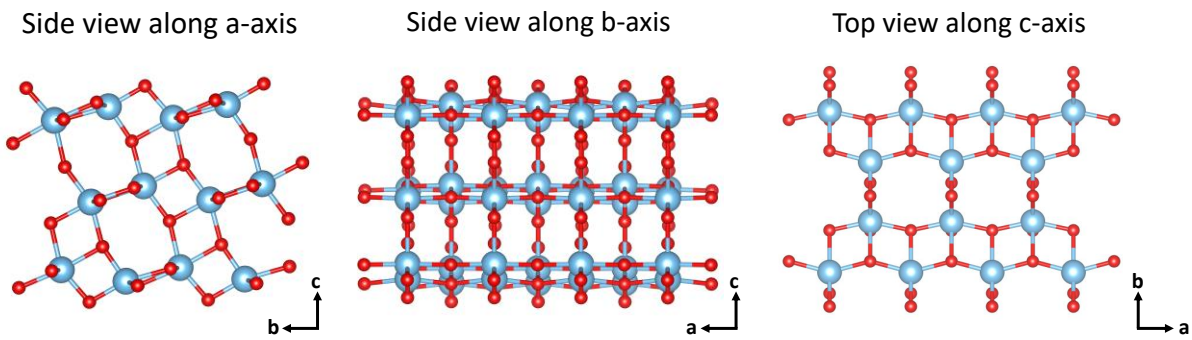

Figure 1. General overview of the (101) anatase surface slab model.

Adsorption of Single *d*-Metal Atoms on the (101) Anatase Support

The adsorption of single Group 8-10 metal atoms on the anatase support (a' = 11.58 Å, b' = 10.48 Å and c' = 30.76 Å; vacuum layer of 20 Å) was subsequently investigated following the computational approach indicated in the previous section. During the optimisation of these models all ionic positions were allowed to fully relax, with a convergence criterion for the energy of 10^{-8} eV and a Gaussian smearing width of 0.001 eV. The adsorption energy of the single metal atom is given by Equation 1 where E(M), E(S) and E(M/S) correspond respectively to the energy of the free metal atom, plain anatase surface and supported metal atom.

$$\mathrm{E_{ads}} = \mathrm{E(M/S)} - \mathrm{E(M)} - \mathrm{E(S)} \qquad (1)$$

To assess the role of charge transfer on the adsorption process, the spin density (ρ_s) and effective atomic charges were computed using the Bader decomposition scheme.[26] In order to determine the influence of the Hubbard term on the strength of the adsorption and the parameters affecting it, we also computed the various models without such correction (Table S3). Since this gives rise to identical trends, but a less accurate description of the band gap as well as a full delocalisation of the spin density, we restrain the subsequent discussion to the data obtained with an effective Hubbard term of 4 eV. The nature of the interactions between the anatase support and transition metals was described using density derived electrostatic and chemical bond orders (DDEC6),[27] and density of states (DOS). The DOS data were obtained from static calculations starting from a previously converged charge density, using 2000 energy grid points and a (15 x 15 x 1) Γ-centred Monkhorst-Pack k-point grid.

Reactivity Indices

Conceptual reactivity indices allowing the characterization of the global and local chemical response of the selected catalytic systems towards electron transfer were computed using the Fermi weighted density of states approach introduced by Zhuang et al.[28] In our earlier work on silica adsorbed single *d*-metal atoms,[14] we showed that this approach is the most appropriate for the accurate description of reactivity indices of periodic systems. This approximation enables both the global (S_F) and local (s_F) Fermi softness to be determined from the integration over a suitable energy range of the product of a weight function and the total ($g(\varepsilon)$) or local ($g(\varepsilon, \vec{r})$) density of states (Equation 2). Because of the discontinuity of the density with respect to the number of electrons,[29] the local Fermi softness is split into an electrophilic (s_F^+) and nucleophilic (s_F^-) part. Hence, the former index is obtained from an integration over the conduction band, which characterizes the addition of an electron to the system. On the other hand, the propensity to electron removal (s_F^-) is derived from an integration with the Fermi level as upper limit. The

weight function, defined as the derivative of the Fermi-Dirac distribution function at a given nominal electron temperature (k_BT), enables to scale the contribution of an energy state to the total reactivity according to its location relative to the Fermi level. The nominal electron temperature, determining the distribution of the weight function, was chosen such that within the energy range of interest each state was assigned a weight factor of at least 0.1%.

$$S_F = \int_{-\infty}^{+\infty} g(\varepsilon) \left(\frac{\partial f(\varepsilon)}{\partial \mu} \right)_v d\varepsilon$$
$$s_F(\vec{r}) = \int_{\mu \pm \delta\mu} g(\varepsilon, \vec{r}) \left(\frac{\partial f(\varepsilon)}{\partial \mu} \right)_v d\varepsilon \quad (2)$$

Adsorption of Carbon Monoxide on TiO_2-Supported *d*-Metal Systems

The models representing the adsorption of a single carbon monoxide molecule on the anatase-supported *d*-metal systems were optimised using the above-mentioned computational procedure. As defined in Equation 3, the adsorption energy was determined as a difference between the energy of the adsorbed complex E(CO/S), the isolated CO molecule E(CO) and the supported metal atom system E(M/S).

$$E_{ads}(CO) = E(CO/S) - E(CO) - E(M/S) \quad (3)$$

The role of back bonding interactions on the adsorption strength was assessed by means of CO stretching frequencies. These frequencies were computed within the harmonic approximation, at the gamma point, in which displacements of the CO molecule and the adsorbed *d*-metal atom in three directions were allowed (± 0.02 Å). The remaining atoms were kept frozen during the frequency calculation. The frequency of an isolated carbon monoxide molecule at the PBE-D3BJ level of theory was used as reference value (2129 cm^{-1}).

Results and Discussion

Adsorption of Single Late *d*-Metal Atoms on the (101) Anatase Support

One of the main concerns regarding the suitability of supported single atoms for catalytic purposes is their possible reduced stability due to the distinctly more mobile character as compared to nanoparticles. In this regard, we first describe the adsorption of single *d*-transition metal atoms from Group 8 (Fe, Ru and Os), Group 9 (Co, Rh and Ir) and Group 10 (Ni, Pd and Pt) on the defect-free (101) anatase support, before characterising their chemical reactivity by means of conceptual DFT indices. Based on already established findings,[11] we restrict this study to one particular binding site, which allows interactions between the *d*-metal and two- or three-fold coordinated oxygen atoms as well as five- or six-fold coordinated titanium atoms of the crystal lattice (Figure 2). According to existing literature,[11] this hollow binding site usually provides the most energetically advantageous interactions. As evidenced from Table S4 (Supporting Information), the DDEC6 bond orders as well as the comparison between the relevant bonding distances and sum of covalent radii indicate that these interactions are polar covalent in nature. The adsorption energies of the different metals at the binding site are shown in Table 1 (see Figure S5 of the Supporting Information for more details on the optimised geometries of the different transition metals).

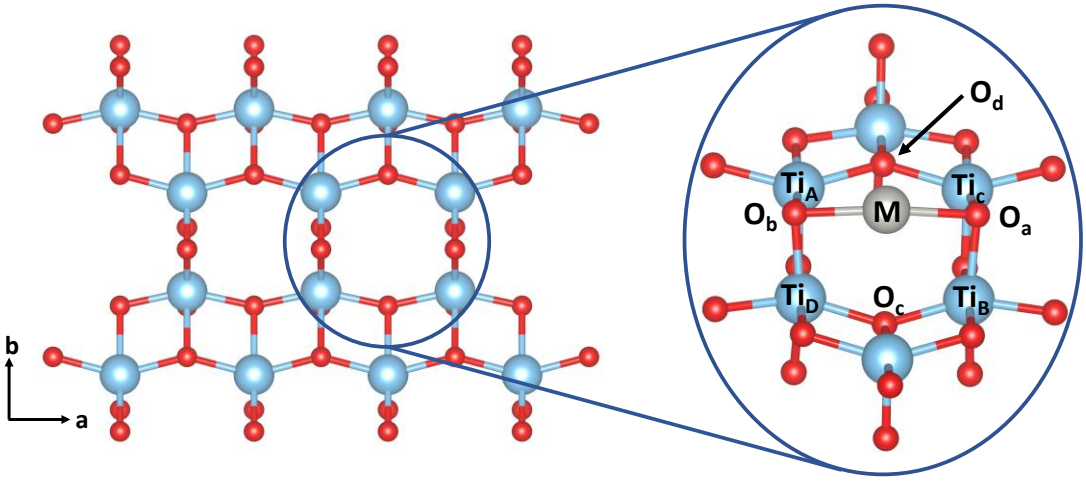

Figure 2. Top view representation of the surface model together with the considered hollow binding site.

The adsorption energies of the late *d*-transition metal atoms indicate a strong interaction with the anatase surface (Table 1). The majority of the investigated atoms are characterized by adsorption energies varying between -3.11 eV (Rh) and -3.50 eV (Ir), with two exceptions; Os and Pd. The osmium atom interacts significantly stronger with the TiO_2 surface (E_{ads} = -3.80 eV), while in analogy with our previous study on the amorphous silica surface,[14] the adsorption of the Pd atom is much weaker (E_{ads} = -1.99 eV) as compared to the remaining metal atoms. Evidence for this different behaviour of Pd is also experimentally retrieved as the dissociation enthalpy of a Pd-O bond was established at 2.47 eV, a remarkably lower value as compared to the ones found for the other M-O bonds ranging from 3.79 eV for Ni-O to 5.96 eV for Os-O.[31] Besides this link with experiment, our adsorption energies display periodic trends throughout the periodic table of elements. As such, with the exception of Fe and Co, Figure 3b indicates a decreasing trend in adsorption energy (less negative values) when successive elements belonging to the same row are considered. Within one group, the row 5 metal interacts weaker as compared to the row 4 or 6 element. In contrast, the relative difference in adsorption strength between rows 4 and 6 is overall rather small. These trends in adsorption energies coincide entirely with the amount of available unpaired *d* electrons that can interact with the oxygen atoms of the oxide support. Whereas within a row the number of unpaired *d* electrons decreases for increasing atomic numbers, the observations within a group turn out to be related to a different way of populating the orbitals. Hence, except for the Pt atom, the different electrons of row 4 and row 6 *d*-metal atoms will be distributed according to Hund's rule and the Aufbau principle or Klechkowsky's rule. This gives rise to row 4 and 6 electronic configurations that are similar within a group and consist of a maximum of unpaired *d* electrons. In contrast, the orbital filling of the row 5 transition metal atoms forms an exception to these rules as one or both of the energetically lower n*s* electrons already reside in the valence *d* shell, thereby reducing the number of unpaired *d* electrons.

Table 1. Adsorption energies of anatase-supported Group 8-10 transition metal atoms at the hollow binding site along with the Bader charges, Mulliken electronegativity, magnetic moments and spin densities on both the metal and the support.

	E_{ads}[a]	q_M[b]	χ_M[c]	$\lvert\mu_M\rvert$[d]	$\lvert\mu_{M/S}\rvert$[e]	$\rho_{s,M}$[f]	$\rho_{s,Ti}$[g]
Fe	-3.43	1.06	4.06	4.00	4.00	3.33	0.90
Ru	-3.14	0.73	4.50	4.00	2.00	0.93	0.90
Os	-3.80	0.65	4.90	4.00	2.00	0.79	0.92
Co	-3.44	0.78	4.30	3.00	3.00	1.97	0.89
Rh	-3.11	0.59	4.30	3.00	1.00	0.00	0.90
Ir	-3.50	0.57	5.40	3.00	1.00	0.00	0.89
Ni	-3.26	0.70	4.40	2.00	2.00	0.86	0.89
Pd	-1.99	0.16	4.45	0.00	0.00	0.00	0.00
Pt	-3.17	0.07	5.60	2.00	0.00	0.00	0.00

[a]Adsorption energy (in eV); [b]Net Bader charges of the metal atoms adsorbed on the support (in I*e*I); [c]Mulliken electronegativity of the free metal atom[30] (in eV); [d]Magnetic moment of free metal atoms (in μ_B); [e]Magnetic moment of M/TiO_2 systems (in μ_B); [f]Spin density on the adsorbed transition metal (in I*e*I); [g]Spin density on the titanium atom of the binding site (in I*e*I).

Furthermore, these results are in good agreement with a previous study on the adsorption of early, middle and late transition metal atoms on the anatase surface by Deskins et al.[11e] This study established that the late elements interact generally weaker with the anatase support than the early transition metals. For instance, their calculations provided adsorption energies of -6.70 eV (Sc), -4.96 eV (V), -3.37 eV (Mn), -3.13 eV (Co), and -2.31 eV (Cu) for the Group 3-5-7-9-11 series, which corresponds to a decrease of 4.39 eV in interaction strength between Group 3 and Group 11. The adsorption energies for the single Fe, Ru, Rh, Pd and Pt system reported by Deskins are very similar to our computations, as respective values of -3.42 eV, -3.19 eV, -3.11 eV, -2.03 eV and -3.24 eV were revealed.[11e] In addition to the position of the element in the periodic table, the same authors reported a good correlation (R^2 = 0.78) between the Bader charges on the adsorbed transition metal and its adsorption strength.[11e] Accordingly, they found that the higher this charge was, the stronger the metal interacted with the oxygen atoms of the surface. The electron transfer from the adsorbed metal to the support is an inherent consequence of the reducible nature of the anatase surface and this correlation suggests its importance for the stability of single *d*-metal atoms on oxide supports.

The above-mentioned findings are corroborated when comparing the adsorption energies and Bader charges for the anatase surface with the values in our previous paper on the amorphous silica surface (Figure 3). Amorphous silica is a typical example of a non-reducible surface, which minimises the charge transfer as much as possible. In this regard, Figure 3 highlights a distinct increase in both the interaction strength and accompanied Bader charge on the transition metal when this metal interacts with the anatase surface instead. For instance, the adsorption of the considered row 4 elements (Fe, Co, Ni) on the silica surface is associated with an energy of -1.40, -1.78 and -1.92 eV,[14] respectively, whereas on the anatase surface the interaction is significantly stronger, resulting in adsorption energies of -3.43, -3.44 and -3.26 eV. Simultaneously, the Bader charges for these anatase-supported row 4 transition metal atoms are twice as high as compared to the non-reducible surface, which confirms the favourable influence of an electron transfer process on the adsorption strength. This increase in electron transfer from the metal towards the oxide support is even more pronounced for the heavier row 5 and 6 elements, as their Bader charges are a factor of four to six higher with respect to silica. Moreover, in contrast to silica, all metals are characterized

by positive charges and hence transfer of electrons occurs from the metal towards the support. Despite the marked numerical differences in Bader charges between the anatase and silica surface, very similar periodic trends are obtained.

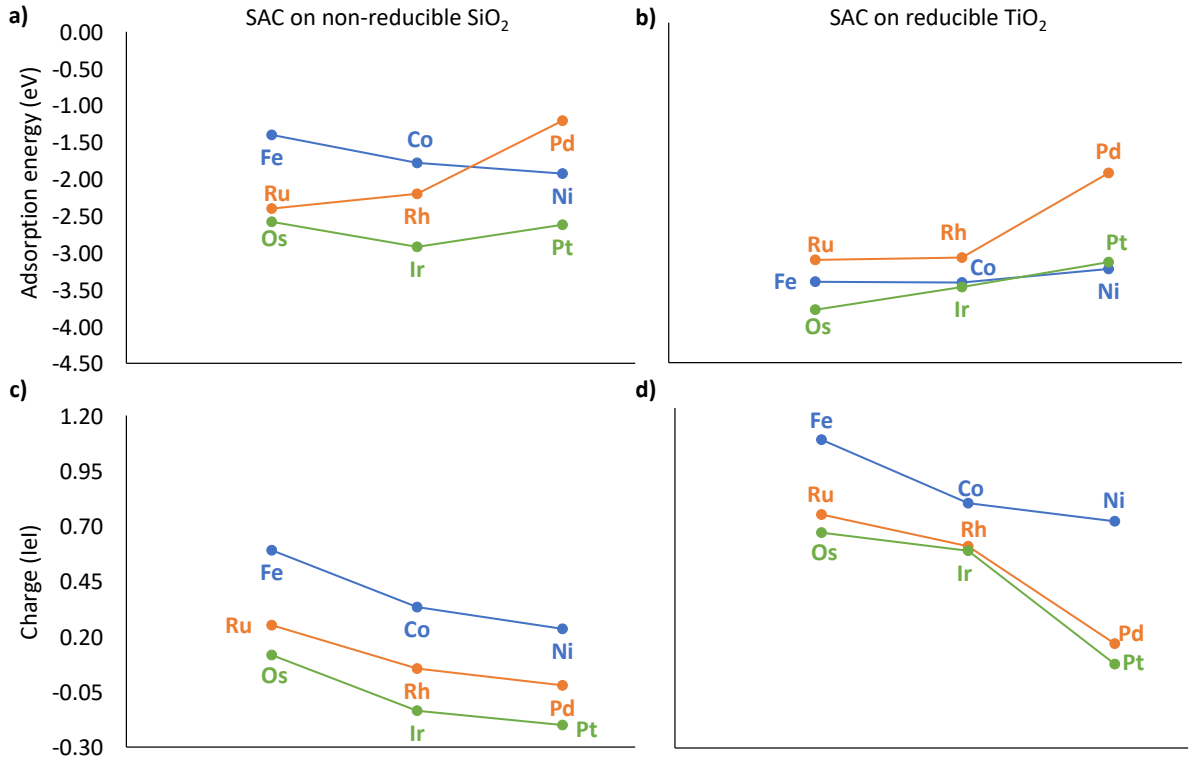

Figure 3. Adsorption energies (in eV) of late transition metals on the non-reducible silica (a) and reducible anatase (b) support; Bader charges (in |*e*|) of the silica- (c) and anatase-supported (d) late transition metals.

The charge on the TiO_2-adsorbed transition metal atom shows a decreasing trend throughout a period and across a group, a tendency consistent with the Mulliken electronegativity of the respective transition metals (Table 1). Correspondingly, the least electronegative element from the investigated series, the Fe atom (χ_M = 4.06 eV), carries the largest Bader charge (q_M = 1.06 |e|) and is responsible for the largest transfer of electrons towards the anatase surface. Analogously, the most electronegative Pt atom (χ_M = 5.60 eV) appears to be the least prone to charge transfer given its low charge of 0.07 |e|. In our investigation on the silica support, we assessed that the more the transition metal was inclined to donate electrons (i.e. low electronegativity and high Bader charge), the weaker its adsorption energy was due to the non-reducible nature of the support.[14] However, the opposite reasoning, implying that the larger the Bader charge on the transition metal, the stronger the interaction with the anatase surface should be, does not appear to hold for these late transition metal atoms. For instance, the charge on the Pt atom is ten times smaller (q_M = 0.07 |*e*|) with respect to the Ni atom (q_M = 0.70 |*e*|), yet the adsorption of both metals on anatase is characterised by almost identical energies of -3.17 and -3.26 eV. Notwithstanding the favourable influence of the reducible character of the support on the strength of the interaction with the transition metal atom, the very poor correlation factor of 0.34 indicates that the adsorption strength of single late transition metal atoms cannot solely be attributed to the magnitude of the charge transfer.

In order to provide additional insight into the observed adsorption trends we focus on the spin density (ρ_s) distribution as well as magnetic moment differences between the system after metal adsorption $|\mu_{M/S}|$ and its separate entities (free metal atom $|\mu_M|$ and the plain anatase surface $|\mu_S|$). These electronic parameters are summarized in Table 1. All magnetic moments in this table were determined over the entire volume of the unit cell, avoiding the potential underestimation of this quantity due to interstitial spaces related to the Wigner-Seitz spherical model.[32] The computed magnetic moments for the free *d*-transition metals ($|\mu_M|$) were also compared with their ground state spin multiplicities as mentioned in literature.[33] Given the absence of unpaired electrons in the defect-free plain (101) anatase surface a magnetic moment $|\mu_S|$ of 0 μ_B is obtained.

The influence of the electronic parameters on the adsorption of single *d*-metal atoms clearly emerges from the analysis of the Group 10 (Ni, Pd, Pt) elements. As such, it can be noted from Table 1 that, despite the significant difference in energies between Pd (E_{ads} = -1.99 eV) and Pt (E_{ads} = -3.17 eV), the adsorption of these two metals is not influenced by a charge transfer process. The lack of electron transfer from the transition metal to the support is evidently observed from the Bader charges, which are much smaller in comparison with the remaining elements. Accordingly, upon adsorption the single Pd and Pt atoms carry a positive charge of 0.16 and 0.07 l*e*l. Further evidence for this observation is provided by the absence of spin density, defined as the difference between the number of α and β spin electrons, on the reducible support (Figure 4). This is, given the singlet state ($\alpha = \beta$) of the plain anatase surface, a clear indication that no electron was transferred from the metal to the support. However, the total magnetic moment of the system ($|\mu_{M/S}|$) is in both cases found to be zero, while the initial electronic configuration of a free Pd or Pt atom corresponds respectively to a singlet ($|\mu_M|$ = 0 μ_B) and a triplet ($|\mu_M|$ = 2 μ_B) multiplicity. In view of the missing charge transfer, this quenching of the magnetic moment can only be ascribed to the rearrangement of the atomic energy levels of the Pt atom. More precisely, the coordination of the Pt atom with the oxygen atoms of the support triggers the formation of *s-d* hybrid orbitals allowing the promotion of the unpaired 6*s* electron into the 5*d* shell in order to obtain a completely filled outer shell. The positive influence of such a hybridisation effect on the adsorption strength was also observed on non-reducible supports.[13,14]

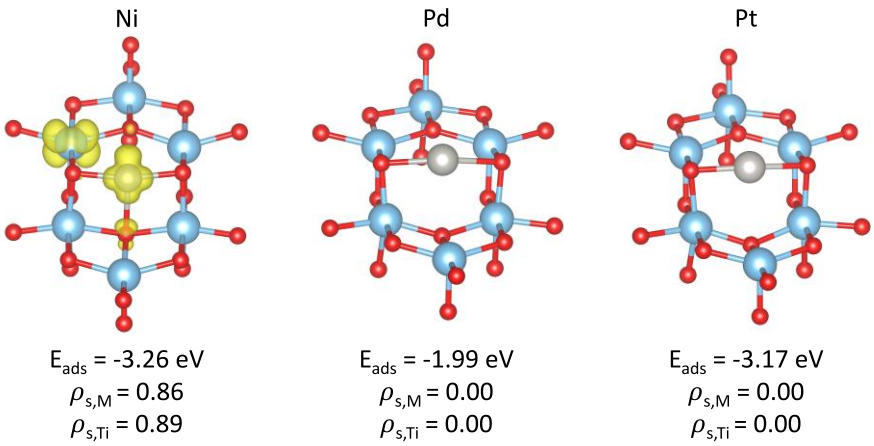

Figure 4. Isosurfaces (isovalue = 0.01 au) representing the localisation of spin density for the anatase-supported Group 10 atoms.

Prior to the description of Ni, it is worth mentioning that as the computational description of the triplet state of Ni ($3d^84s^2$ or $3d^94s^1$) is complex given the extremely small energy difference

between both levels (0.025 eV),[34] the plane-wave GGA description used in this work constrained the configuration of Ni to $3d^9 4s^1$.[13b] Therefore, given the very similar adsorption energies of both Ni and Pt and their computational identical ground state configuration ($3d^9 4s^1$), it would be reasonable to expect an important role of orbital hybridisation on the adsorption of Ni as well. However, unlike Pt, chemisorption of Ni is associated with a Bader charge of 0.70 l*e*l, a ten-fold increase with respect to Pt. Hence, as indicated by the presence of *d* orbital shaped spin density localised around one of the Ti atoms of the support (Figure 4), a clear transfer of the 4*s* electron of the free nickel atom towards anatase occurred. This transfer thereby prevents the formation of *s*-*d* hybrid orbitals and leaves the anatase-supported nickel atom with one unpaired *d* electron as can be observed in Figure 4. Consequently, we conclude that the adsorption of Pt is mainly influenced by a hybridisation effect, whereas for nickel the charge transfer appears to be the main driving force.

In contrast to the Group 10 metal atoms, a synergetic relationship between hybridisation and electron transfer appears to be the crucial factor influencing the adsorption strength of the Group 9 elements (Co, Rh and Ir). In this regard, the chemisorption of Co and Ir on the anatase support yields almost identical adsorption energies of -3.44 and -3.50 eV, whereas the corresponding row 5 element (Rh) interacts less strongly (E_{ads} = -3.11 eV). Despite the energy difference, the spin density ($\rho_{s,Ti} \approx 0.9$) as well as the Bader charges (Table 1) indicate that the charge transfer after chemisorption on the anatase surface occurs in almost identical amounts for both Ir (q_M = 0.57 l*e*l) and Rh (q_M = 0.59 l*e*l). This single electron transfer leaves the anatase support with one unpaired electron in such a way that the total magnetic moment of the system ($|\mu_{M/S}|$ = 1.00 μ_B) can only be reached when all outer shell electrons of both the Ir and Rh atom are paired. The singlet multiplicity of the transition metal seems, at first sight, incompatible with the electronic configuration of the free rhodium ($[Kr]4d^8 5s^1$) and iridium ($[Xe]4f^{14} 5d^7 6s^2$) atom. However, as suggested by Pacchioni,[7c] the oxide support no longer plays an innocent role when the adsorption of small metallic particles is considered and can be regarded as a very bulky ligand. Consequently, similar to homogeneous catalytic complexes, the *d* orbitals of the transition metal are energetically reorganised upon adsorption, causing a loss of degeneracy. This phenomenon is confirmed by our analysis of atomic *d* orbital projections of the various bands near the Fermi level and is schematically illustrated in Figure 5. Here it is shown that after the adsorption of the Rh atom the initial five-fold degeneracy of the *d* orbitals is completely lifted and a splitting diagram in which the $d_{x^2-y^2}$ orbital is higher in energy than the remaining four *d* orbitals is obtained. The 8 *d* electrons of Rh are distributed over the four energetically lower lying *d* orbitals, leaving $d_{x^2-y^2}$ unoccupied. In contrast to Rh, the lifting of the degeneration turns out to be only partial for the adsorbed Ir-system, as the d_{z^2} orbital recedes and aligns with the d_{xz} orbital. Since the energetic gap between the d_{yz} and the $d_{x^2-y^2}$ orbital is still large, the presence of these degenerate states does not affect the distribution of the available electrons. Moreover, as the original electron configuration of Ir obeys Klechkowsky's rules, unlike Rh, this chemisorption process is also accompanied with the promotion of the remaining 6*s* electron to the 5*d* shell and ensuing formation of the *s*-*d* hybrid orbital by analogy with Pt. The stronger adsorption of the row 6 metal again demonstrates the favourable influence of hybridisation, on top of charge transfer. A completely identical reasoning can be applied to the corresponding Group 8 elements, Ru and Os. Consequently, as the orbital filling for Os is similar to Ir, we believe that charge transfer (q_{OS} = 0.65 l*e*l) and hybridisation are at the core of the strong adsorption (E_{ads} = -3.80 eV). In contrast, the electron configuration of Ru deviates

from Klechkowsky's rules and therefore the adsorption energy of -3.14 eV can only be attributed to the charge transfer (q_{Ru} = 0.73 l*e*l).

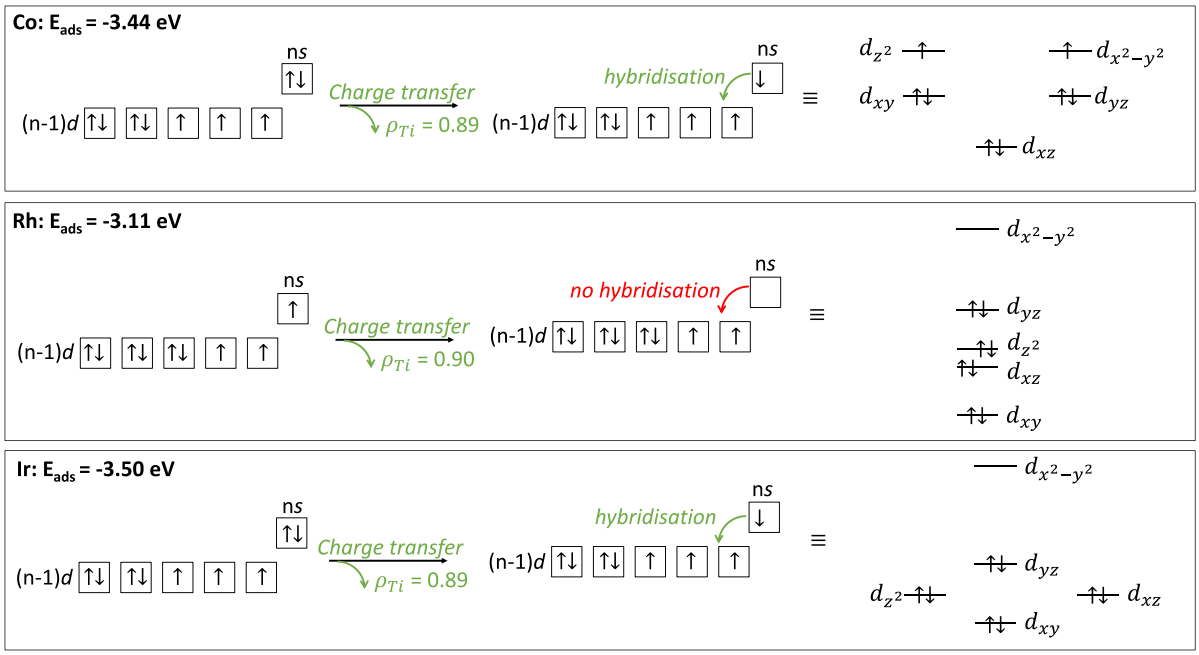

Figure 5. Schematic overview of the different effects influencing the adsorption of Group 9 *d*-metals on the anatase support. Both the occurrence of the hybridisation effect and the orbital splitting was retrieved from our computed atomic orbital projections of the different bands.

Given the similarity in electron configuration between a row 4 and 6 element, both Fe and Co, are not surprisingly influenced by the same electronic features as Os and Ir. However, as evidenced by the larger magnetic moments of these systems, a preference for a high spin state complex upon adsorption is observed. The stronger adsorption of Os (E_{ads} = -3.80 eV) with respect to Fe (E_{ads} = -3.43 eV) is due to the more intense distortions of the anatase surface upon interaction with the former element. In this regard, Deskins et al. evidenced a good correlation between strong adsorption energies and surface fluxionality.[11e]

Reactivity of Anatase Supported Single *d*-Metal Atoms

In this section we go beyond the description of electronic and structural parameters that determine the strength of the interaction with the support. The term "single-atom catalyst" implies more than the adsorption process, since, as the definition indicates, the reactivity of the catalytic complex should arise mainly from the adsorbed metal along with possible contributions from nearby functional groups or atoms of the support. A qualitative approach to confirm this key feature consists in verifying that the orbital contributions in the vicinity of the Fermi level are mainly due to the *d*-metal. As revealed by the density of states (Figures S15-S24 of the Supporting Information), the initial band gap of the anatase support gets populated by new electronic states upon adsorption of the *d*-metal atoms. These higher-energy filled states play an important role in catalytic processes and originate primarily from the *d*-metal, confirming the leading role of the transition metal in the overall reactivity of the system. Alternatively, conceptual DFT indices provide a more quantitative approach towards the assessment of chemical reactivity, without the need of additional complex calculations. In our previous work on the adsorption of single late *d*-transition metals supported on an

amorphous silica surface[14] we investigated the suitability of three conceptual DFT schemes (finite difference approximation, density of states integration and Fermi weighted density of states integration) for the description of the reactivity of such periodic models. We identified the Fermi weighted approach, in which the product of the Fermi-Dirac weight function and the density of states is integrated over a given energy range, as the most appropriate one. Hence, this approach was used to describe the reactivity of our anatase-supported systems.

The application of the global Fermi softness (S_F) as a descriptor for the overall reactivity of these systems requires the definition of a suitable interval of energy states located around the Fermi level. This interval is determined by the nominal electron temperature (k_BT). In this respect, we have evaluated the global Fermi softness for each of the models at various k_BT values ranging from 0.10 to 0.95 eV. The resulting S_F values are summarized in Table S5 of the Supporting Information. Next to the Fermi softness, we subsequently considered the global softness of each system as the inverse of its bandgap. The latter indices are solely dependent on the computational method but do not depend at all on the chosen nominal electron temperature. As both the Fermi softness and global softness values, which were shown to be intrinsically related in our previous paper on amorphous silica,[14] are retrieved from calculations with an identical functional and basis set, we argue that the degree of correlation between these indices should allow the assessment of the most suitable weight distribution function for the systems of interest.

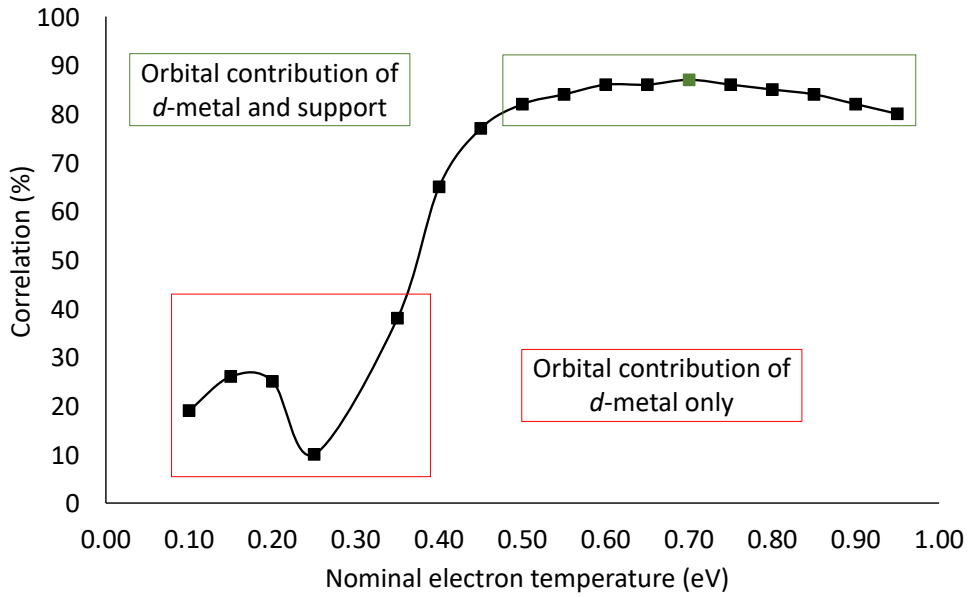

Figure 6. Correlation (R^2) between the global softness evaluated as the inverse of the bandgap and the Fermi softness (y-axis) for nominal electron temperatures ranging between 0.10 and 0.95 eV (x-axis). A narrow weight function that mainly contains orbital contributions from the adsorbed metal shows a poor correlation with the global softness (pink). A larger weight function including both metal and support contributions substantially increases the correlation (green).

The analysis of the correlation (Figure 6) reveals that when the Fermi-Dirac weight function describes a very narrow distribution, and only the highest energy level is considered, no correlation with the band gap exists (pink region). Since integration over this energy level, which almost exclusively contains contributions from the transition metal, leads to such a poor description, we assume that the overall reactivity of these anatase-supported systems

is not only originating from the metal atoms, in contrast to the silica support. This hypothesis is confirmed by the increase in correlation as more weight is given to slightly lower energy levels that contain a given percentage of TiO_2 character. This means that the reducible nature of the support not only enhances the strength of the chemisorption of the *d*-metal, but also influences the total reactivity of the catalytic system. Therefore, systematically increasing the nominal electron temperature up to 0.70 eV causes a steady increase in the correlation factor until a maximum value of 0.87 is reached (green region in Figure 6). The resulting global Fermi softness values for the various systems are listed in Table 3.

Table 3. Summary of the global Fermi softness (eV^{-1}) obtained through the weighted density of states approach at a nominal electron temperature of 0.70 eV.

Group 8	S_F	Group 9	S_F	Group 10	S_F
Fe/TiO_2	26.15	**Co/TiO_2**	27.24	**Ni/TiO_2**	25.60
Ru/TiO_2	22.93	**Rh/TiO_2**	23.38	**Pd/TiO_2**	24.29
Os/TiO_2	24.10	**Ir/TiO_2**	23.03	**Pt/TiO_2**	22.26

In comparison with the global reactivity of our previously studied M/SiO_2 systems,[14] the obtained global Fermi softness (S_F) values for the anatase-supported single-atom systems are significantly higher. This more pronounced availability for charge transfer related processes can be attributed primarily to the reducible character of the Ti^{4+} atoms of anatase. Furthermore, the band gap of a pure anatase surface (3.2 eV) is significantly smaller than that of amorphous silica (ca. 9 eV), which eases the transfer of electrons towards the conduction band as a smaller energy barrier needs to be crossed. From Table 3, it can be observed that the highest S_F values are obtained for the systems consisting of the row 4 elements (Fe, Co and Ni). Despite the difference in magnitude, this trend was also observed for the amorphous silica surface. The high softness of the adsorbed Fe and Co on anatase is related to the high spin state of the transition metal and consequent larger number of unpaired electrons in the valence band. In the case of Ni, the high propensity to charge transfer is due to the fact that after adsorption this metal is only missing one electron to reach the stable d^{10} configuration.

In addition to the global reactivity picture, the local Fermi softness allows for a more targeted focus on the propensity towards electron uptake or release of well-defined areas of the surface. As the active site is the most relevant for catalytic purposes, the next discussion is devoted to the reactivity of this region. The local Fermi softness for the active sites at a nominal electron temperature of 0.70 eV is summarized in Table 4. Besides the adsorbed transition metal atom, we also consider the Ti atoms of the hollow binding site as possible members of the active site. In the previous section, we have observed that the transition metal atom carries a partial positive charge after adsorption on the anatase surface, which shows a decreasing trend throughout successive periods and groups. From a chemical reactivity point of view, this means that the adsorbed *d*-metal behaves like a Lewis acid and is hence exposed to the interaction with a Lewis base. The degree to which this *d*-metal is sensitive to this process can best be described by the local softness for electron addition (s_M^+) index. Table 4 reveals that this index is the largest for the adsorbed row 4 *d*-metals and systematically decreases for the heavier transition metals within the same group. This trend is also noticed when elements from the same row are compared. Thus, the tendencies in local softness for nucleophilic attack are fully aligned with the trends in partial charge (Figure 7),

which implies that the metals that were most subject to charge transfer towards the support tend to be overall more prone to accommodate incoming negative charge.

Table 4. Local Fermi softness (in a.u. eV^{-1}) obtained through the weighted density of states approach at a nominal electron temperature of 0.70 eV along with the Bader charges (in |*e*|) on the corresponding atoms.

	q_M	s_M^+	Δq_{Ti_A} [a]	$s_{Ti_A}^+$	$s_{Ti_A}^-$	Δq_{Ti_B} [a]	$s_{Ti_B}^+$	Δq_{Ti_C} [a]	$s_{Ti_C}^+$	Δq_{Ti_D} [a]	$s_{Ti_D}^+$
Fe/TiO₂	1.06	0.46	0.27	0.03	0.23	0.21	0.10	0.01	0.23	0.00	0.27
Ru/TiO₂	0.73	0.32	0.28	0.01	0.25	0.15	0.05	0.06	0.09	0.01	0.06
Os/TiO₂	0.65	0.20	0.28	0.02	0.24	0.19	0.08	0.10	0.09	0.00	0.14
Co/TiO₂	0.78	0.29	0.26	0.03	0.23	0.06	0.31	0.00	0.30	0.02	0.21
Rh/TiO₂	0.59	0.16	0.29	0.01	0.26	0.05	0.11	0.06	0.08	0.01	0.07
Ir/TiO₂	0.57	0.03	0.31	0.01	0.26	0.07	0.11	0.08	0.07	0.02	0.09
Ni/TiO₂	0.70	0.16	0.27	0.02	0.25	0.03	0.25	0.02	0.18	0.01	0.12
Pd/TiO₂	0.16	0.02	0.03	0.15	0.03	0.03	0.15	0.03	0.15	0.03	0.15
Pt/TiO₂	0.07	0.00	0.03	0.01	0.04	0.04	0.00	0.03	0.01	0.04	0.00

[a]Difference between the net Bader charge of the Ti before and after adsorption of the transition metal atom.

Next to the adsorbed transition metal, the effect of the charge transfer on the reactivity of the surrounding Ti atoms of the hollow binding site can also be assessed from their corresponding local reactivity index. Indeed, the local softness for electron addition for titanium atom Ti_A (Figure 2) is described by a significantly lower value than the remaining three Ti atoms. Based on the analysis of spin density, we assessed that Ti_A corresponds to the atom on which most of the charge transfer is localized. This suggests that Ti_A occurs in a reduced Ti^{3+} state instead of the expected Ti^{4+} state. The resulting small s_M^+ values correlate with a reduction potential of -0.9 V and a thermodynamically non-favourable process associated with the further reduction to Ti^{2+}. In contrast, the local softness for electrophilic attack (s_M^-), which corresponds to an electron removal or oxidation process, is significantly higher for Ti_A. At first glance, this observation may seem contradictory, as the reducible character of the TiO_2 surface has been mentioned throughout this paper as a trigger for the strong adsorption and higher reactivity compared to a non-reducible amorphous silica surface. However, the Latimer diagram for titanium shows that the transition from Ti^{4+} to Ti^{3+} is described by a small, positive reduction potential of approximately 0.1 V. This reaction is thermodynamically favourable, though the Gibbs free energy associated with it is expected to be rather low. This allows us to hypothesise that the higher s_M^- values for the Ti_A atom can be traced back to the fact that the reduction of Ti^{4+} to Ti^{3+} is a strongly reversible process. For the remaining Ti atoms ($Ti_{B\text{-}D}$), which accumulate significantly less spin density, the opposite picture applies - the less charge they absorb, and thus the more Ti^{4+} character they exhibit, the greater the local softness for nucleophilic attack (Table 4) and the smaller the local softness for electrophilic attack (Table S6 of the Supporting Information). The surrounding Ti atoms can thus be considered an explicit part of the active site, as they can serve both as electron donors and acceptors.

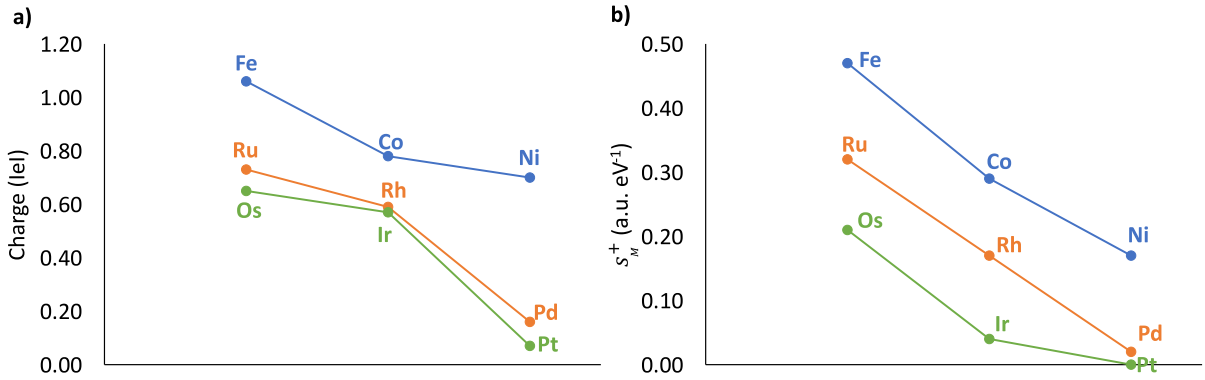

Figure 7. a) Bader charges (in l*e*l) of the anatase-supported late transition metal atoms (a) and their corresponding local softness values (in a.u. eV^{-1}) for electron addition (b).

CO Adsorption on TiO_2-Supported Single *d*-Metal Atoms

Carbon monoxide (CO) is a highly relevant Lewis base adsorbate that recently gained a lot of interest as it constitutes the first intermediate in the activation of CO_2, a serial catalytic hydrogenation process resulting into alcohols and longer hydrocarbon chains. However, this process is only conceivable if the desorption of CO is energetically less advantageous than the subsequent hydrogenation.[35] Consequently, a deep understanding of the factors affecting the interaction strength is required. In the last part of this paper, we present preliminary results on the adsorption of one CO molecule on the anatase-adsorbed *d*-metal atom and assess the suitability of reactivity indices for predictive purposes. The adsorption energy of this probe molecule on the single Group 8-10 transition metal atoms is summarized in Table 5, whereas the optimised geometries are depicted in Figure S25 of the Supporting Information. This table shows that the adsorption energy of a CO molecule on row 4 elements (Fe, Co, Ni) fluctuates between -1.17 (Fe) and -1.62 eV (Ni). These values are significantly lower than in the case of heavier transition metal atoms (row 5 and 6). With an adsorption energy of respectively -2.87 and -2.91 eV, the strongest interaction with the CO molecule is found for the Ru and Ir systems. The chemisorption of CO on the remaining elements (Os, Rh, Pt) is, with the exception of Pd, characterized by a relatively similar adsorption energy ranging between -2.35 (Rh) and -2.50 eV (Pt). Aside from the significantly weaker interaction between CO and row 4 elements, no clear trends could be identified within the periodic table.

On the other hand, our computed adsorption energies do agree with the experimentally assessed selectivity of the CO_2 hydrogenation reaction towards either CO or CH_4 over TiO_2-supported late transition metals. Considering the CO molecule to be the first intermediate product of the CO_2 activation reaction and methane to be obtained from its subsequent hydrogenation, we argue that an experimentally high selectivity for CO refers to a small computed CO adsorption energy (row 4), whereas a stronger CO chemisorption (i.e. more negative E_{ads}) preferentially leads to high amounts of CH_4. In this context single Ni atoms dispersed on a TiO_2 support revealed for a wide range of reaction temperatures a 99% selectivity for the CO product, whereas under similar reaction conditions the selectivity of single Ru atoms on TiO_2 appeared to be fully shifted towards methane.[36] Alternatively, the hydrogenation of CO_2 over titania-supported small Rh clusters (2 wt%) yields 72.7% of CH_4, while CO was obtained as major product (73%) when using small Fe clusters (2.5 wt%).[37] A pronounced preference for methane was also established for smaller Rh/TiO_2 systems[38] (1 wt%) as well as Ir/TiO_2 catalytic systems.[39]

Table 5. Adsorption energy of a CO molecule on TiO_2-supported Group 8-10 transition metal atoms along with the CO stretching frequency, relevant bond lengths (d_{C-M}) and Bader charges.

	E_{ads}[a]	ν_{CO}[b]	$\Delta\nu_{CO}$[c]	d_{C-M}[d]	$\sum_{cov}$	q_M[e]	Δq_M[f]	q_{CO}[g]
Fe	-1.17	1980	-149	1.75	2.08	0.97	-0.09	-0.23
Ru	-2.87	1941	-188	1.82	2.22	0.60	-0.13	-0.28
Os	-2.47	1941	-188	1.83	2.20	0.81	+0.16	-0.33
Co	-1.47	2004	-125	1.71	2.02	0.78	0.00	-0.16
Rh	-2.35	2000	-129	1.81	2.18	0.61	+0.02	-0.14
Ir	-2.91	2006	-123	1.82	2.17	0.63	+0.06	-0.20
Ni	-1.62	2046	-83	1.75	2.00	0.78	+0.08	-0.15
Pd	-1.97	2022	-107	1.83	2.15	0.22	+0.06	-0.18
Pt	-2.50	2025	-104	1.80	2.12	0.08	+0.01	-0.10

[a]Adsorption energy (in eV); [b]CO stretching frequency (in cm^{-1}); [c] CO frequency shift (in cm^{-1}) with respect to a reference value of non-interacting CO (2129 cm^{-1}); [d]Metal-carbon distance (in Å); [e]Net Bader charges of the metal atoms upon adsorption of CO (in I*e*I); [f]Difference in charge on the metal prior to and after adsorption of the CO molecule (in I*e*I); [g]Net Bader charge of the adsorbed CO molecule (in I*e*I).

This motivates us to assess the driving forces behind the CO adsorption based on the previously established insights. In this context, we have revealed that upon adsorption on the anatase support the transition metal atom is characterised by a partial positive charge. Hence, the chemisorption of a CO molecule on these systems should be considered as an interaction between a Lewis acid and base, which is essentially composed of an electrostatic, covalent and polarisation contribution. The importance of the electrostatic component can be assessed using molecular electrostatic potentials (MEPs). These are generated with respect to a proton and show electron rich or poor regions. An electron poor region, corresponding to a positive electrostatic potential (V_{max}), is expected to be a suitable anchor point for the CO molecule. Indeed, Stenlid et al.[40] noted a stronger adsorption of a CO molecule on small TiO_2 clusters when the maximal electrostatic potential of these supporting systems increased.[41] According to their model, this Lewis acidity descriptor is perfectly capable to retrieve the adsorption energy trends (R^2 = 0.96). Nevertheless, the adsorption of CO on TiO_2 clusters as well as on the anatase surface is extremely weak, as maximal adsorption energies of -0.71 eV[40] and -0.34 eV,[41] respectively, are reported. These values are significantly lower than those obtained for our systems and this might explain why neither the maximum electrostatic potential of the whole system (R^2 = 0.04), nor the local potential of the adsorbed transition metal (R^2 = 0.07) corroborates with the computed adsorption energy.

Given the larger number of available *d* electrons in the considered late transition metals as compared to titanium, the absence of a purely electrostatically driven CO adsorption process is not unexpected. The strength of the CO ligand is, besides the σ bond between the metal and the free electron pair on carbon, often ascribed to its very distinct π back bonding properties. This requires an overlap between filled *d* orbitals of the metal in a low oxidation state and the LUMO of CO, which results in a strengthened metal-carbon bond and a decrease in the characteristic CO stretching frequency. Both the red shift of the CO frequency as the shortening of the distance between the metal and carbon atom was evidenced for all our systems (Table 5). It should, nevertheless, be mentioned that the quantitative strength of back bonding with the PBE functional may be overestimated, as the crucial $2\pi^*$ orbital of CO is systematically characterized by a too low energy with this functional.[42] Notwithstanding this shortcoming of PBE, we qualitatively confirm the presence of the back bonding properties

and therefore believe that a good predictive model for CO adsorption on anatase-supported *d*-metal atoms require indices able to retrieve such a charge transfer process.

The global Fermi softness (S_F), which describes the propensity of the entire system towards charge transfer, constitutes a good starting point and reveals a correlation of 80% with adsorption energies (Figure 8). These energies can now within a 95% probability interval (P=0.001) be estimated using the following general equation:

$$\mathrm{E_{ads}} = 0.33\mathrm{S_F} - 10.24 \quad (4)$$

It can be seen that the strength of the interaction between the CO molecule and the adsorbed transition metal atom increases as the overall softness of the entire system decreases. Since the CO molecule is characterised by a hardness value that is very similar to that of well-known hard molecules such as NH_3,[30] this trend is in line with the Hard & Soft Acids and Bases principle, which states that a hard base preferentially interacts with a harder system.

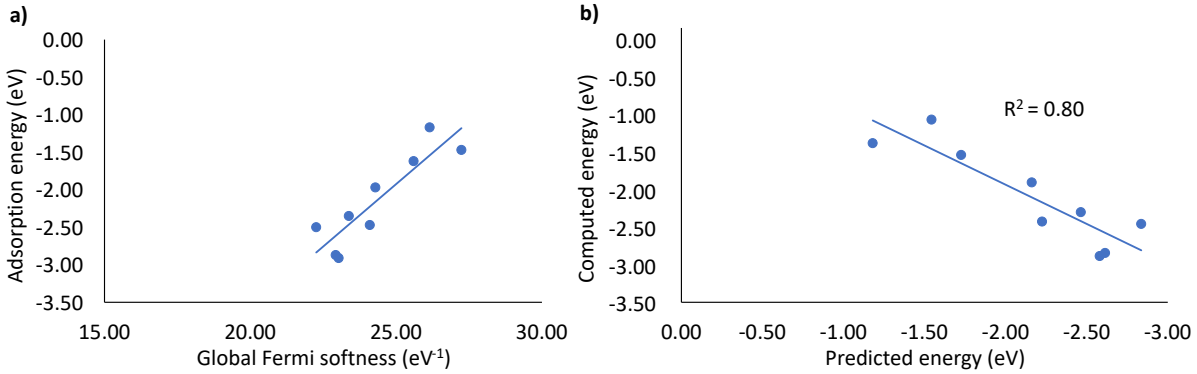

Figure 8. a) Correlation plot between the global Fermi softness (in eV^{-1}) and the CO adsorption energies (in eV). b) Correlation between computed adsorption energies and predicted values (in eV) obtained from a regression model containing the global Fermi softness as single variable.

Considering that CO adsorption is expected to be mainly limited to the active site, the next step consists of switching to a more localised form of this model. Herein, the bonding contribution to the adsorption energy originating from the transfer of the free electrons on carbon towards the *d*-metal can be assessed using the transition metal's local softness for electron addition (s_M^+) index, while the back-bonding can be taken into account by means of the local softness for electron removal (s_M^-) index. The resulting regression model (Figure 9) shows an extremely weak correlation of 37% and does not allow us, at first glance, to accurately predict the adsorption energy. However, in Figure 9a, which depicts the correlation between our calculated adsorption energies and these predicted values, one value (red point) catches our attention because of its rather dissimilar behaviour as compared to the others. Excluding this outlier (Ru) significantly increases the correlation of the regression model up to a value of 0.84. The local density of states of the Ru system (Figure S7) indicates that several peaks originating from the metal *d*-orbitals are distributed over a narrow energy range around the Fermi level. As the indices used in this predictive model are obtained from an integration over this interval, we hence assume that the deviating behaviour might be ascribed to an improper projection of the orbitals of Ru near the Fermi level. The adjusted model allows, within the 95% probability interval (P=0.01), to describe the adsorption energy of CO as:

$$\mathrm{E_{ads}} = 0.92\mathrm{s_M^-} + 5.03\mathrm{s_M^+} - 4.30 \quad (5)$$

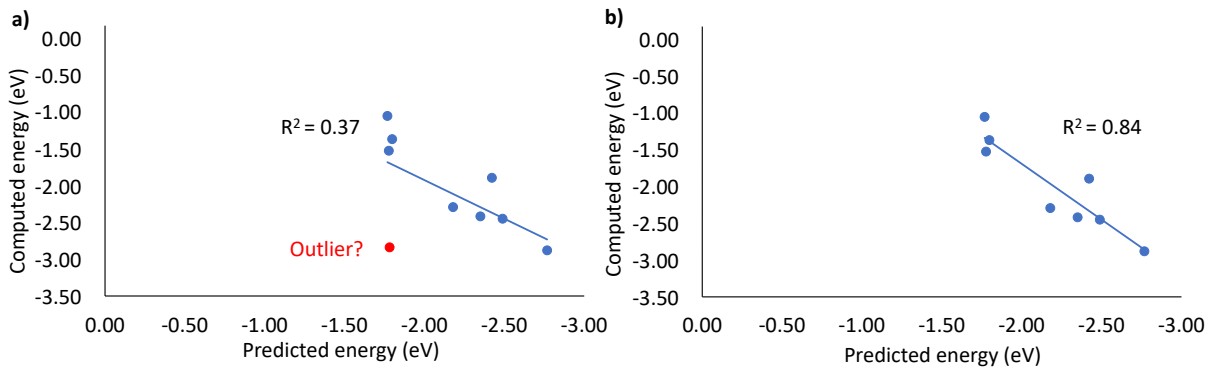

Figure 9. a) Correlation between computed adsorption energies and predicted values (in eV) obtained from a multiple regression model containing the metal's local Fermi softness for nucleophilic and electrophilic attack as variables; b) Correlation between computed adsorption energies and predicted values (in eV) obtained from the same model, excluding a potential outlier.

This model performs slightly better than the model described by Equation 4, which only includes the global Fermi softness. A further improvement lies in introducing indices belonging to the surrounding atoms of the active site. This idea is supported by the comparison between the total negative charge on the CO molecule (q_{CO}) and the difference in Bader charge on the transition metal before and after CO chemisorption (Δq_M). If, as assumed in the model described by Equation 5, the adsorption only concerns an interaction between the initially electropositive *d*-metal atom and the CO molecule, then q_{CO} and Δq_M should cancel each other out. From Table 5, it can be noticed that although most of the metal atoms carry a larger positive charge upon CO adsorption, Δq_M represents only a small fraction of q_{CO}. Thus, we believe that the surrounding Ti and O atoms of the support also actively participate in the CO adsorption process. Since our current set of energies without the outlier is restricted to 8 CO adsorbed systems, introducing additional variables into the model could lead to an overparametrized situation. Therefore, it seems more reasonable to first extend our dataset by considering more systems before searching for a more appropriate prediction model, which will be the subject of future work.

Conclusion

Based on periodic DFT calculations, the influence of various electronic effects on the interaction strength between late transition metal atoms and the hollow binding site of a defect-free (101) anatase surface was assessed. The interaction is characterised by adsorption energies ranging, except for Pd, between -3.11 (Rh) and -3.80 eV (Os). The strength of these interactions is linked to the position of the metal in the periodic table. Hence, a *d*-metal of row 5 interacts systematically weaker with the surface, whereas the interaction between anatase and a row 4 or 6 transition metal of the same group is described by an almost identical adsorption energy. This observation is attributable to the initial orbital filling of the considered elements and more precisely to the number of unpaired *d* electrons. Metals obeying Klechkowsky's rule (rows 4 and 6), and therefore containing a larger number of unpaired *d* electrons, interact more strongly than metals for which orbital filling constitutes an exception to this principle (row 5). However, independent of the amount of unpaired *d* electrons, the adsorption energies are always significantly higher than those obtained for adsorption on a non-reducible oxide surface, confirming the favourable influence of charge transfer on the adsorption strength. Due to the very poor correlation between the computed Bader charges on the *d*-metal atoms and their adsorption energies ($R^2 = 0.34$), we assess that

the strength of the chemisorption cannot be solely attributed to the magnitude of the charge transfer. This is clearly reflected in the analysis of the TiO_2-adsorbed Pt atom, revealing strong adsorption (-3.17 eV) along with a small Bader charge (q_M = 0.07 lel). Therefore, the strong adsorption between Pt and the anatase surface results mainly from a stabilising *s-d* hybridisation effect allowing the metal to adopt a d^{10} configuration upon adsorption. In contrast, the chemisorption of Ni, which has the same electron configuration as Pt, is exclusively driven by a strong electron transfer (-0.70 lel) despite a very similar adsorption energy of -3.24 eV. Charge transfer was also found to play a major role for Rh and Ru, while for the remaining Group 8 and 9 metal atoms the influence of this effect was further enhanced by *s-d* orbital hybridisation. This synergetic effect is enabled by the Klechkowsky-based orbital filling of these elements, which ensures that the (n+1)*s* orbital still contains one unpaired electron after charge transfer. In summary, three major effects were defined as the driving forces behind the strong adsorption. Process on anatase being *i*) electron transfer towards anatase, *ii*) *s-d* orbital hybridisation, or *iii*) a combination of both factors.

Next, the reactivity of the studied systems was evaluated using the Fermi weighted density of states approach. The resulting values for the global Fermi softness (S_F) were significantly higher than those obtained for the amorphous silica systems and confirm the importance of the reducible character of the support not only on the adsorption strength but also on the reactivity. The highest propensity towards charge transfer processes was obtained for the anatase-supported row 4 metals, with values of 26.15 (Fe), 27.24 (Co) and 25.60 eV^{-1} (Ni). For Fe and Co, these observations were attributed to the adopted high spin electronic configuration, whereas for the Ni/TiO_2 system the pronounced soft character is related to the tendency to achieve a stable d^{10} configuration by uptake of only one electron. In addition to the global Fermi softness, the highest values for the local softness for nucleophilic attack (s_M^+) were also retrieved for row 4 metals. This index showed a completely identical trend as the net Bader charge on the metal and indicated that the more positively charged the metal atom is, the more inclined it is to electron addition. Moreover, the local indices allowed us to determine that the surrounding Ti atoms of the hollow binding site should be considered as a part of the active site since they can serve both as electron donors and acceptors. As such, the Ti atom containing the majority of the spin density upon adsorption, which is now formally in an oxidation state of +III, is described by a very small local softness for nucleophilic attack (s_{Ti}^+), but remarkably higher local softness for electrophilic attack (s_{Ti}^-). In contrast, the opposite trend is noticed for the remaining Ti^{4+} atoms. This implies that the reduction of Ti^{4+} towards Ti^{3+} can be considered as a reversible process, while further reduction to Ti^{2+} seems rather unlikely. These findings are supported by the standard reduction potentials for such reactions.

Finally, a model allowing to predict the adsorption energy of a single carbon monoxide molecule on the adsorbed *d*-metals was constructed. By assessing the red shift in CO stretching frequency as well as the shortening of the carbon-metal bond lengths, we qualitatively showed the crucial role of back bonding in the adsorption of CO. This type of interaction corresponds to a charge transfer process and hence requires a model that relies on conceptual reactivity indices. Our model, in which the local Fermi softness of the transition metals for both nucleophilic and electrophilic attack were included as the only variables, revealed a correlation of 84% with respect to the calculated adsorption energies when a possible outlier was neglected.

Acknowledgements
The authors wish to thank the Vrije Universiteit Brussel (VUB) for the continuous support and in particular the funding through a Strategic Research Program. M.A. and J.T. would like to acknowledge the financial support of the Research Foundation-Flanders (Project No. 12F4416N and 12Y7718N). The computational resources and services used in this work were provided by the VSC (Flemish Supercomputer Center), funded by the Research Foundation Flanders (FWO) and the Flemish Government – department EWI.

Keywords: anatase, charge transfer, density functional calculations, reactivity indices, transition metals.

References

[1] G. Rothenberg, *Catalysis: concepts and green applications*, Wiley-VCH, Weinheim, **2017**, 2nd Edition, p. 320.

[2] Z. Ma, F. Zaera, *Heterogeneous Catalysis by Metals in Encyclopedia of Inorganic Chemistry*, (Eds.: R.B. King, R.H. Crabtree, C.M. Lukehart, D.A. Atwood), John Wiley & Sons, Hoboken, New Jersey, **2006**, DOI: 10.1002/9781119951438.eibc0079

[3] J.R. Ludwig, C.S. Schindler, *Chem.* **2007**, *2*, 313-316.

[4] B. Qiao, A. Wang, X. Yang, L.F. Allard, Z. Jiang, Y. Cui, J. Liu, J. Li, T. Zhang, *Nat. Chem.* **2011**, *3*, 634-641.

[5] a) X.-F. Yang, A. Wang, B. Qiao, J. Li, J. Liu, T. Zhang, *Acc. Chem. Res.* **2013**, *46*, 1740-1748; b) J. Liu, *ACS Catal.* **2017**, *7*, 34-59; c) L. Liu, A. Corma, *Chem. Rev.* **2018**, *118*, 4981-5079; d) A. Wang, J. Li, T. Zhang, *Nat. Rev. Chem.* **2018**, *2*, 65-81; e) H. Zhang, G. Liu, L. Shi, J. Ye, *Adv. Energy Mater.* **2018**, *8*, 1701343; f) F. Chen, X. Jiang, L. Zhang, R. Lang, B. Qiao, *Chinese J. Catal.* **2018**, *39*, 893-898. And references therein.

[6] S. Mitchell, E. Vorobyeva, J. Pérez-Ramirez, *Angew. Chem. Int. Ed.* **2018**, *57*, 15316-15329.

[7] a) J.R. Croy, S. Mostafa, J. Liu, Y. Soh, H. Heinrich, B.R. Cuenya, *Catal. Lett.* **2007**, *119*, 209-216; b) J.A. Farmer, C.T. Campbell, *Science* **2010**, *329*, 933-936; c) G. Pacchioni, *Phys. Chem. Chem. Phys.* **2013**, *15*, 1737-1757; d) M. Ahmadi, H. Mistry, B.R. Cuenya, *J. Phys. Chem. Lett.* **2016**, *7*, 3519-3533; e) T.W. van Deelen, C.H. Meija, K.P. de Jong, *Nat. Catal.* **2019**, *2*, 955-970.

[8] a) A.L. Linsebigler, G.Q. Lu, J.T. Yates, *Chem. Rev.* **1995**, *95*, 735-758; b) K.I. Hajiivanov, D.G. Klissurski, *Chem. Soc. Rev.* **1996**, *25*, 61-69; c) T. Luttrell, S. Halpegamage, J. Tao, A. Kramer, E. Sutter, M. Batzill, *Sci. Rep.* **2014**, *4*, 4043.

[9] a) U. Diebold, *Surf. Sci. Rep.* **2003**, *48*, 53-229; b) T.B. Ghosh, S. Dhabal, A.K. Datta, *J. Appl. Phys.* **2003**, *94*, 4577-4582; c) D.A.H. Hanaor, C.C. Sorrell, *J. Mater. Sci.* **2011**, *46*, 855-874.

[10] a) R.K. Dhokale, H.M. Yadav, S.N. Achary, S.D. Delekar, *Appl. Surf. Sci.* **2014**, *303*, 168-174; b) A.S. Piskun, J. Ftouni, Z. Tang, B.M. Weckhuysen, P.C.A. Bruijnincx, H.J. Heeres, *Appl. Catal., A* **2018**, *549*, 197-206; c) T. Hengsawad, T. Jindarat, D.E. Resasco, S. Jongpatiwut, *Appl. Catal., A* **2018**, *566*, 74-86; d) N. Gogoi, G. Borah, P.K. Gogoi, T.R. Chetia, *Chem. Phys. Lett.* **2018**, *692*, 224-231; e) F. Lin, X. Jiang, N. Boreriboon, Z. Wang, C. Song, K. Cen, *Appl. Catal., A* **2019**, *585*, 117210; f) N.J. Divins, E. Lopez, I. Angurell, S. Neuberg, R. Zapf, G. Kolb, J. Llorca, *Catalysts* **2020**, *10*, 1028; g) X. Chen, H. Wang, M. Chen, X. Qin, H. He, C. Zhang, *Appl. Catal., B* **2021**, *282*, 119543.

[11] a) Y. Han, C. Liu, Q. Ge, *J. Phys. Chem. B* **2006**, *110*, 7463-7472; b) J.F. Sanz, A. Marquez, *J. Phys. Chem. C* **2007**, *111*, 3949-3955; c) J. Zhang, M. Zhang, Y. Han, W. Li, X. Meng, B. Zong, *J. Phys. Chem. C* **2008**, *112*, 19506-19515; d) Z. Helali, A. Markovits, C. Minot, M. Abderrabba, *Struct. Chem.* **2012**, *23*, 1309-1321; e) S.K. Iyemperumal, T.D. Pham, J. Bauer, N.A. Deskins, *J. Phys. Chem. C* **2018**, *122*, 25274-25829.

[12] A. Figueroba, G. Kovacs, A. Bruix, K.M. Neyman, *Catal. Sci. Technol.* **2016**, *6*, 6806-6813.

[13] a) I. Yudanov, G. Pacchioni, K. Neyman, N. Rösch, *J. Phys. Chem. B* **1997**, *101*, 2786-2792; b) A. Markovits, M.K. Skalli, C. Minot, G. Pacchioni, N. Lopez, F. Illas, *J. Chem. Phys.* **2001**, *115*, 8172-8177; c) A. Markovits, J.C. Paniagua, N. Lopez, C. Minot, F. Illas, *Phys. Rev. B* **2003**, *67*, 115417; d) L. Xiao, W.F. Schneider, *Surf. Sci.*, **2008**, *602*, 3445-3453; e) C.K. Narula, G.M. Stocks, *J. Phys. Chem. C* **2012**, *116*, 5628-5636. f) P. Schlexer, G. Pacchioni, *Top. Catal.* **2017**, *60*, 459-470.

[14] X. Deraet, J. Turek, M. Alonso, F. Tielens, S. Cottenier, P.W. Ayers, B.M. Weckhuysen, F. De Proft, *Chem. Eur. J.* **2021**, *27*, 6050-6063.

[15] R.T. Downs, M. Hall-Wallace, *Am. Mineral.* **2003**, *88*, 247-250.

[16] a) G. Kresse, J. Hafner, *Phys. Rev. B* **1993**, *47*, 558-561; b) G. Kresse, J. Hafner, *Phys. Rev. B* **1994**, *49*, 14251-14269; c) G. Kresse, J. Furthmuller, *Comput. Mater. Sci.* **1996**, *6*, 15-50; d) G. Kresse, J. Furthmuller, *Phys. Rev. B* **1996**, *54*, 11169-11186.

[17] a) P.E. Blöchl, *Phys. Rev. B* **1994**, *50*, 17953-17979; b) G. Kresse, D. Joubert, *Phys. Rev. B* **1999**, *59*, 1758-1775.

[18] J.K. Burdett, T. Hughbanks, G.J. Miller, J.W. Richardson, J.V. Smith, *J. Am. Chem. Soc.* **1987**, *109,* 3639-3646.

[19] a) J.P. Perdew, K. Burke, M. Ernzerhof, *Phys. Rev. Lett.* **1996**, *77*, 3865-3868; b) J.P. Perdew, K. Burke, M. Ernzerhof, *Phys. Rev. Lett.* **1997**, *78*, 1396.

[20] a) S. Grimme, J. Antony, S. Ehrlich, H. Krieg, *J. Chem. Phys.* **2010**, *132,* 154104; b) S. Grimme, S. Ehrlich, L. Goerigk, *J. Comput. Chem.* **2011**, *32*, 1456-1465.

[21] I. Urdaneta, A. Keller, O. Atabek, J.L. Palma, D. Finkelstein-Shapiro, P. Tarakeshwar, V. Mujica, M. Calatayud, *J. Phys. Chem. C* **2014**, *118,* 20688-20693.

[22] S.L. Dudarev, G.A. Botton, S.Y. Savrasov, C.J. Humphreys, A.P. Sutton, *Phys. Rev. B* **1998**, *57,* 1505-1509.

[23] F. Birch, *Phys. Rev.* **1947**, *71,* 809-824.

[24] H.J. Monkhorst, J.D. Pack, *Phys. Rev. B* **1976**, *13*, 5188-5192.

[25] M.E. Arroyo-de Dompablo, A. Morales-Garcia, M. Taravillo, *J. Chem. Phys.* **2011**, *135*, 054503.

[26] a) G. Henkelman, A. Arnaldsson, H. Jonsson, *Comput. Mater. Sci.* **2006**, *36*, 354-360; b) E. Sanville, S.D. Kenny, R. Smith, G. Henkelman, *J. Comput. Chem.* **2007**, *28*, 899-908; c) W. Tang, E. Sanville, G. Henkelman, *J. Phys. Condens. Matter.* **2009**, *21*, 084204.

[27] a) T.A. Manz, N.G. Limas, *RCS Adv.* **2016**, 6, 47771-47801; b) N.G. Limas, T.A. Manz, *RCS Adv.* **2016**, 6, 45727-45747; c) T.A. Manz, *RCS Adv.* **2017**, 7, 45552-45581.

[28] B. Huang, L. Xiao, J. Lu, L. Zhuang, *Angew. Chem. Int. Ed.* **2016**, *55*, 6239-6243.

[29] J.P. Perdew, R.G. Parr, M. Levy, J.L. Balduz, *Phys. Rev. Lett.* **1982**, *49*, 1691-1694.

[30] R.G. Pearson, *Inorg. Chem.* **1988**, *27*, 734-740.

[31] *Molecular Structure and Spectroscopy in CRC Handbook of Chemistry and Physics,* 95th edition (Ed.: W.M. Haynes), CRC Press, New York, **2014**, pp 1515-1624.

[32] a) E. Wigner, F. Seitz, *Phys. Rev.* **1933**, *43*, 804-810; b) E. Wigner, F. Seitz, *Phys. Rev.* **1934**, *46*, 509-524.

[33] G.V. Samsonov in *Atomic Structure and Crystallochemical Properties of the Elements in Handbook of Physicochemical Properties of the Elements*, 1st edition (Ed.: G.V. Samsonov), IFI/ Plenum, New York – Washington, **1968**, pp 7-130.
[34] C.E. Moore, *Atomic Energy Levels as Derived from the Analyses of Optical Spectra*, Volume II, U.S. National Bureau of Standards, Washington D.C., **1971**, p. 274.
[35] W. Li, H. Wang, X. Jiang, J. Zhu, Z. Liu, X. Guo, C. Song, *RCS Adv.* **2018**, *8*, 7651-7669.
[36] C. Rivera-Carcamo, C. Scarfiello, A.B. Garcia, Y. Tison, H. Martinez, W. Baaziz, O. Ersen, C. Le Berre, P. Serp, *Adv. Mater. Interfaces* **2021**, *8*, 2001777.
[37] M.R. Gogate, R.J. Davis, *Catal. Commun.* **2010**, *11*, 901-906.
[38] F. Cao, N. Gong, Z. Ma, X. Wang, M. Tan, Y. Wu, Y. Tan, *Chem. Commun.* **2022**, *58*, 4219-4222.
[39] Y. Zhang, Z. Zhang, X. Yang, R. Wang, H. Duan, Z. Shen, L. Li, Y. Su., R. Yang, Y. Zhang, X. Su, Y. Huang, T. Zhang, *Green. Chem.* **2020**, *22*, 6855-6861.
[40] J.H. Stenlid, A.J. Johansson, T. Brinck, *J. Phys. Chem. C* **2017**, *121*, 27483-27492.
[41] H.V. Thang, G. Pacchioni, *J. Phys. Chem. C* **2019**, *123*, 7271-7282.
[42] a) A. Gil, A. Clotet, J.M. Ricart, G. Kresse, M. Garcia-Hernandez, N. Rösch, P. Sautet, *Surf. Sci.* **2003**, *530*, 71-87; b) H.V. Thang, F. Maleki, S. Tosoni, G. Pacchioni, *Top. Catal.* **2021**, DOI: 10.1007/s11244-021-01514-0.

TOC

A CDFT prophecy. Periodic conceptual DFT reactivity indices were computed for a variety of single anatase-supported late transition metal atoms and included into a statistical relevant model predicting the strength of the interaction between these systems and a CO molecule.